Supporting Information for "Lagrangian Eddy Trapping Fosters Chlorophyll Hot Spots in the North Pacific Subtropical Gyre"

DOI: 10.1002/

Alexandra E. Jones[1,2], Michael J. Follows[1]

[1]Department of Earth, Atmospheric, and Planetary Sciences, Massachusetts Institute of Technology, Cambridge, MA, USA

[2]Biology Department, Woods Hole Oceanographic Institution, Woods Hole, MA, USA

Contents of this file

Table S1. Cumulative contributions to chl-a from 2000-2019 8-day averages[a]

	Chl-a $(mg \cdot m^{-3})$	Fraction of Domain Chl-a	Area (km^2)	Fraction of Domain Area	$\frac{1}{\sum_i A_i} \sum_i Chl_i \cdot A_i$ $(mg \cdot m^{-3})$
Domain	23,035,545	100%	6,790,256,191	100%	0.0671
Outside-eddy	19,083,498	82.880%	5,613,465,829	82.669%	0.0671
Anti RCLV	620,088	2.692%	181,066,346	2.667%	0.0678
Anti SLA	1,656,661	7.192%	487,216,799	7.175%	0.0672
Cyc RCLV	711,649	3.089%	214,517,840	3.159%	0.0661
Cyc SLA	1,711,740	7.431%	516,342,064	7.604%	0.0659

[a] Does not include area covered by clouds where chl-a is unknown.

Table S2. Number of pixels with available chl-a in each anticyclonic feature type.[a]

	Anti SLA	Anti RCLV	Anti SLA excluding RCLVs	% of Anti SLA data in RCLVs
Full Domain (all seasons)	24,611,335	9,145,426	19,472,926	20.88%
North Winter	2,573,257	888,074	2,154,500	16.27%
North Spring	2,989,498	1,233,772	2,297,869	23.14%
North Summer	3,537,936	1,482,487	2,675,426	24.38%
North Fall	3,035,172	1,059,554	2,498,944	17.67%
Southeast Winter	1,314,247	411,546	1,115,867	15.09%
Southeast Spring	1,374,094	456,698	1,120,926	18.42%
Southeast Summer	1,925,764	644,587	1,511,821	21.50%
Southeast Fall	1,658,451	544,226	1,356,411	18.21%
Lee Winter	1,599,300	639,110	1,218,971	23.78%
Lee Spring	1,347,659	522,509	1,055,755	21.66%
Lee Summer	1,648,147	636,421	1,249,902	24.16%
Lee Fall	1,607,810	626,442	1,216,534	24.34%

[a] Does not include area covered by clouds where chl-a is unknown.

Table S3. Number of pixels with available chl-a in each cyclonic feature type.[a]

	Cyc SLA	Cyc RCLV	Cyc SLA excluding RCLVs	% of Cyc SLA data in RCLVs
Full Domain (all seasons)	25,960,826	10,758,238	19,943,322	23.18%
North Winter	2,369,956	784,780	2,015,018	14.98%
North Spring	2,438,519	1,036,121	1,986,213	18.55%
North Summer	3,257,596	1,247,902	2,604,223	20.06%
North Fall	2,678,662	895,421	2,263,668	15.49%
Southeast Winter	2,055,452	957,498	1,474,531	28.26%
Southeast Spring	2,072,384	977,892	1,434,013	30.80%
Southeast Summer	2,451,786	1,265,777	1,608,160	34.41%
Southeast Fall	2,057,854	1,046,325	1,441,224	29.96%
Lee Winter	1,383,511	519,921	1,105,519	20.09%
Lee Spring	1,607,596	709,743	1,185,369	26.26%
Lee Summer	1,981,864	772,515	1,499,457	24.34%
Lee Fall	1,605,646	544,343	1,325,927	17.42%

[a] Does not include area covered by clouds where chl-a is unknown.

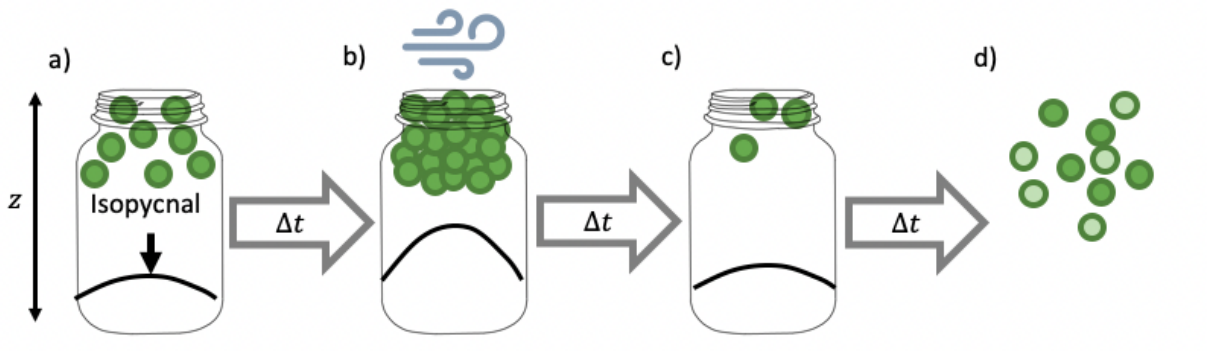

Figure S1. Schematic of the "hot spot" hypothesis. Here a jar is a metaphor for a perfect Rotationally Coherent Lagrangian Vortex (RCLV) where there is no exchange between the eddy and surrounding waters. **a)** The eddy spins up, and an initial phytoplankton population is trapped in the eddy. **b)** A phytoplankton bloom may occur in response to an environmental perturbation and is subsequently trapped and localized within the eddy bounds. **c)** A bloom decay or negative biological response would also be trapped in the vortex due to dilution limitation. **d)** When the eddy loses coherency, the in-eddy population mixes and interacts with the outside-eddy population.

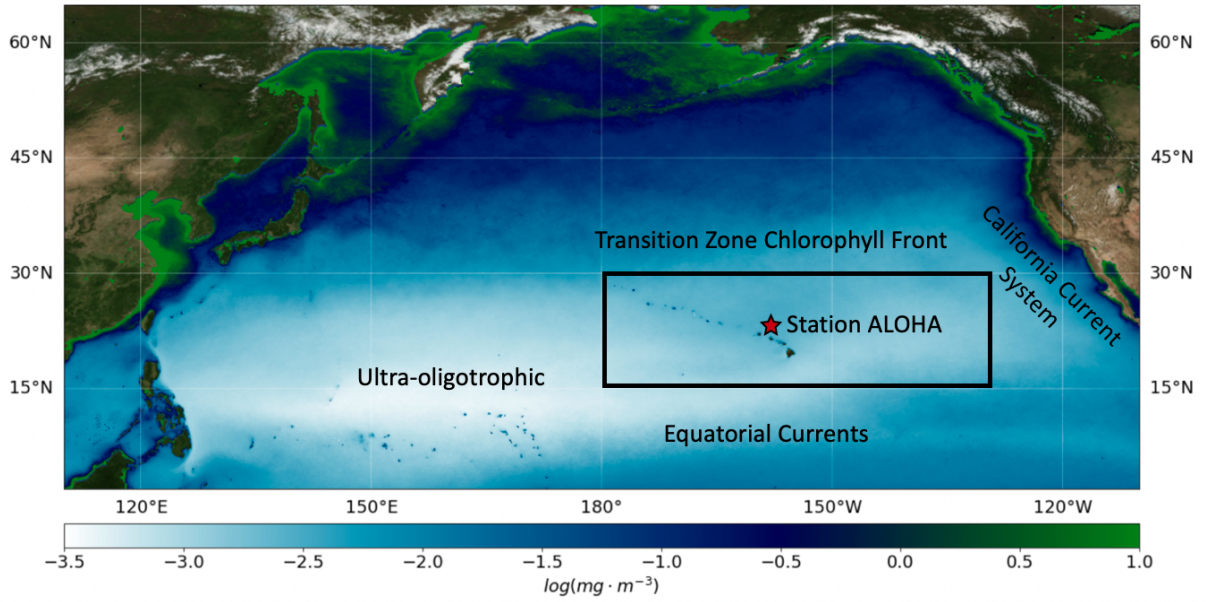

Figure S2. Average surface satellite chl-*a* from 2010-2020 in the North Pacific. The solid black box delineates the domain of this study.

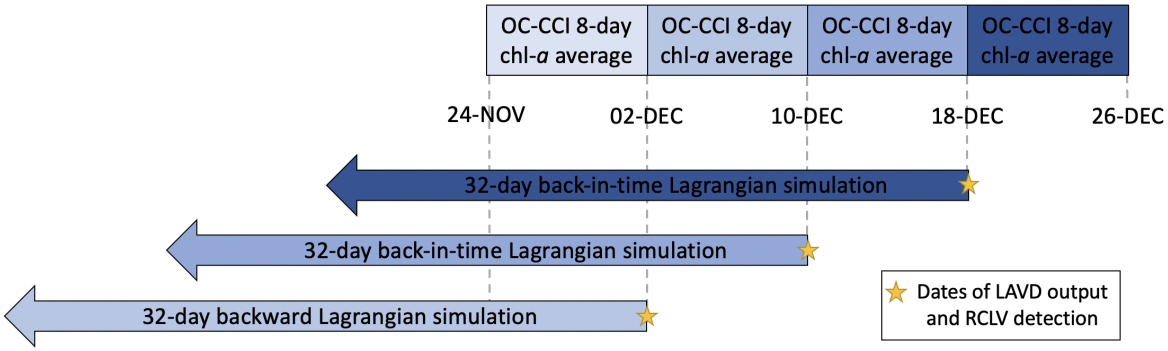

Figure S3. Temporal alignment between 32-day backward-in-time Lagrangian trajectories, RCLV detection, and the 8-day average OC-CCI observations. The blue colors match the RCLV detection dates and the collocated chlorophyll-a 8-day averages.

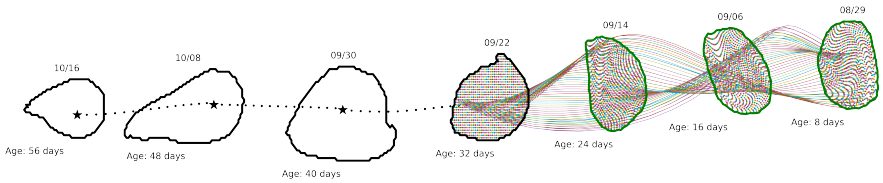

Figure S4. The [Jones-Kellett and Follows 2023] dataset tracked RCLVs forward in time starting with age 32 (date 09/22), shown in black. To simulate the RCLV genesis, we tracked Lagrangian particles contained with 32-day-old RCLVs backward-in-time. The green contours were drawn around the particle sets to represent the RCLV boundaries at ages 24 (09/14), 16 (09/06), and 8 days old (08/29).

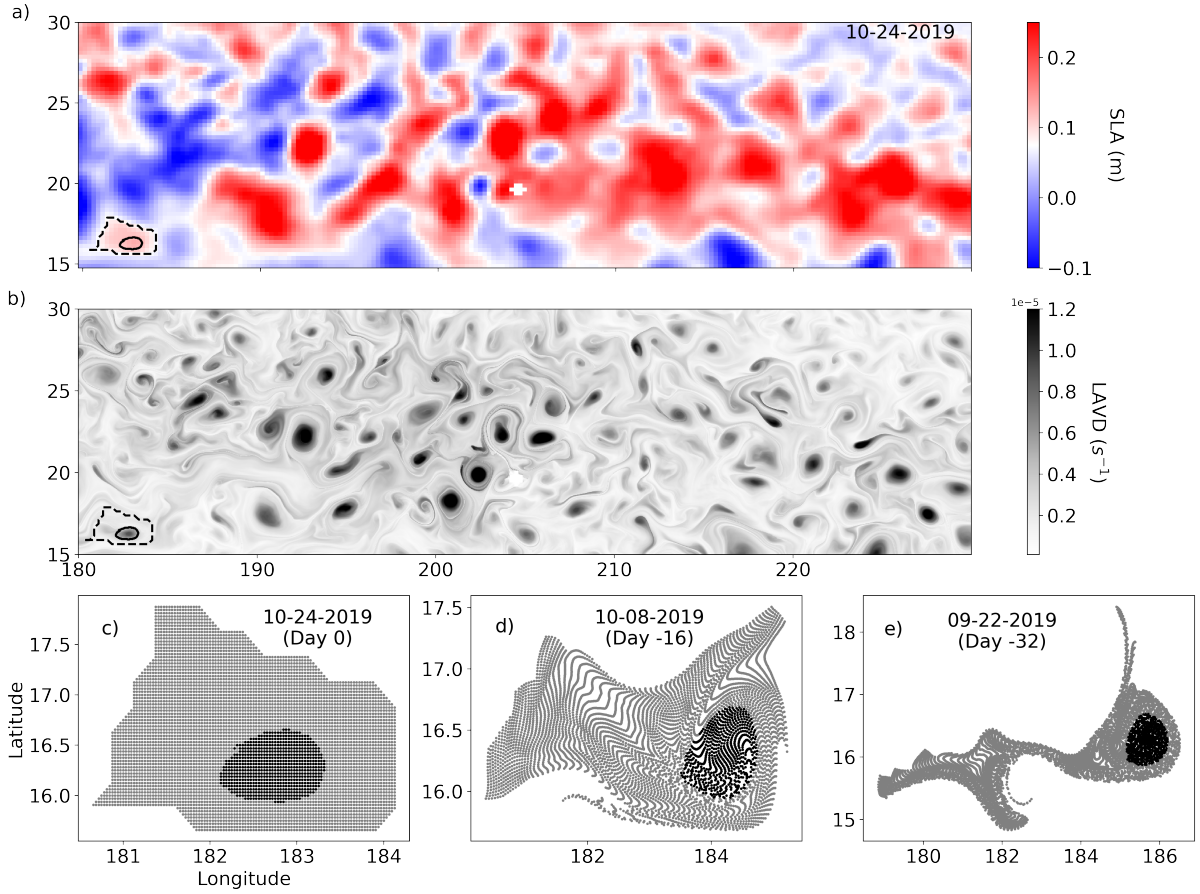

Figure S5. An eddy on October 24th, 2019, with boundaries overlaid on the a) SLA and b) LAVD fields. The black dotted line represents the SLA eddy boundary, and the black solid line is the RCLV boundary. c) Initialization of the Lagrangian particles contained inside the SLA (gray and black) and RCLV (black) boundaries on October 24th, 2019. In this study, the gray particles are categorized as "SLA excluding RCLV". d) The particle locations after advection 16 days backward-in-time and e) 32 days backward-in-time.

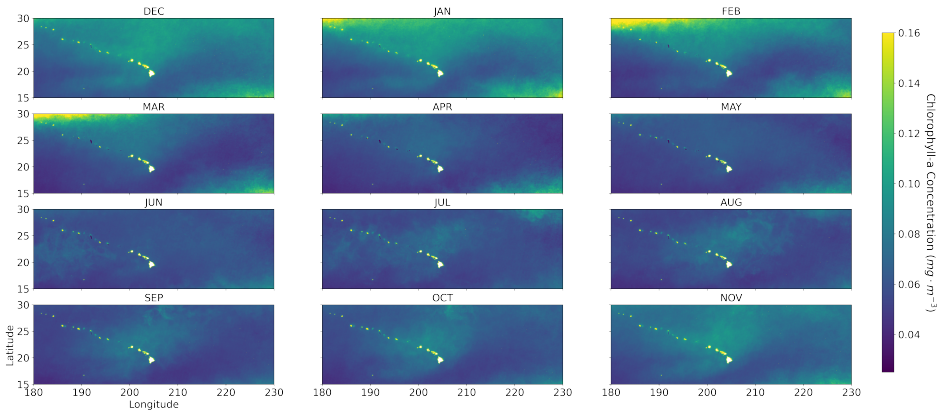

Figure S6. Monthly mean chl-*a* derived from 2000-2019 OC-CCI 8-day averages.

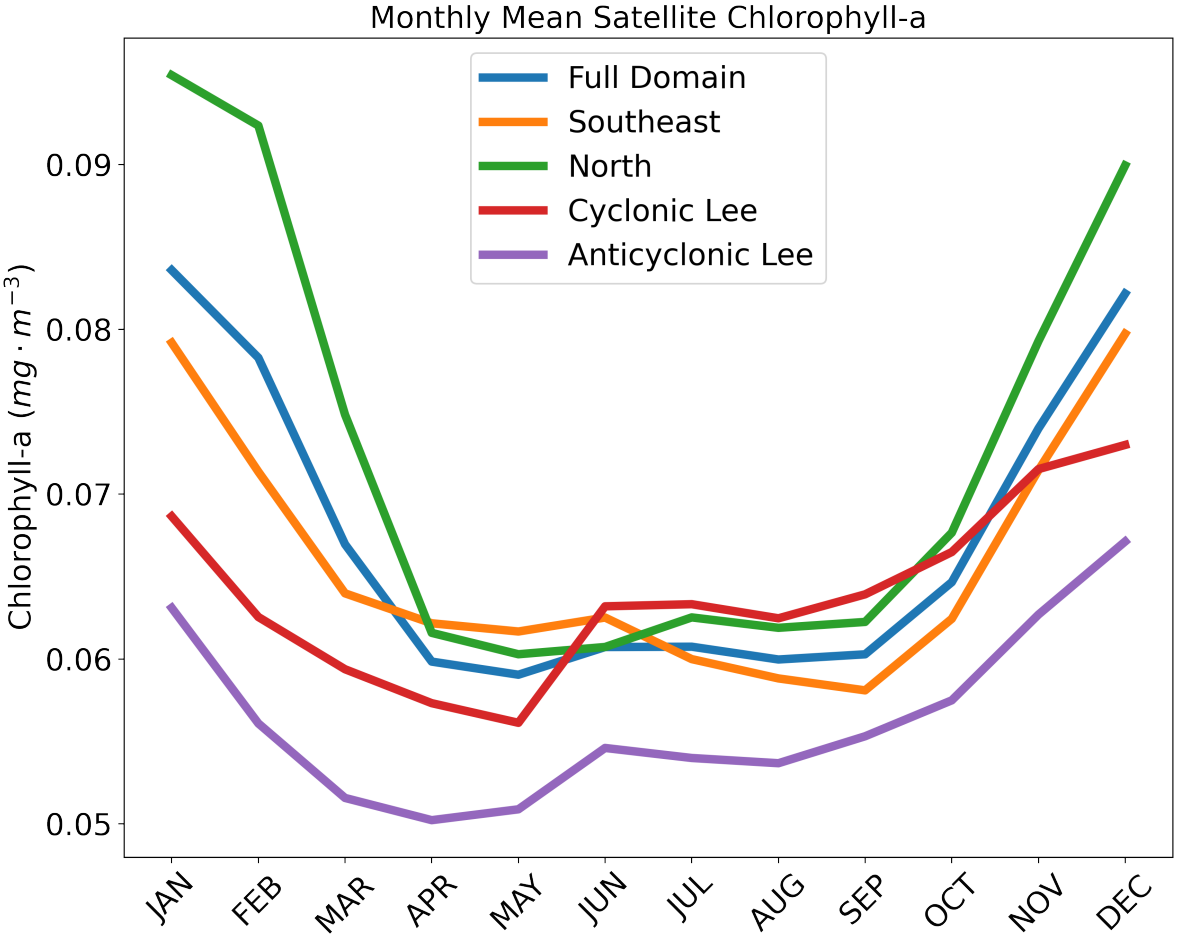

Figure S7. Monthly mean chl-a by province, calculated from 2000-2019 OC-CCI 8-day averages.

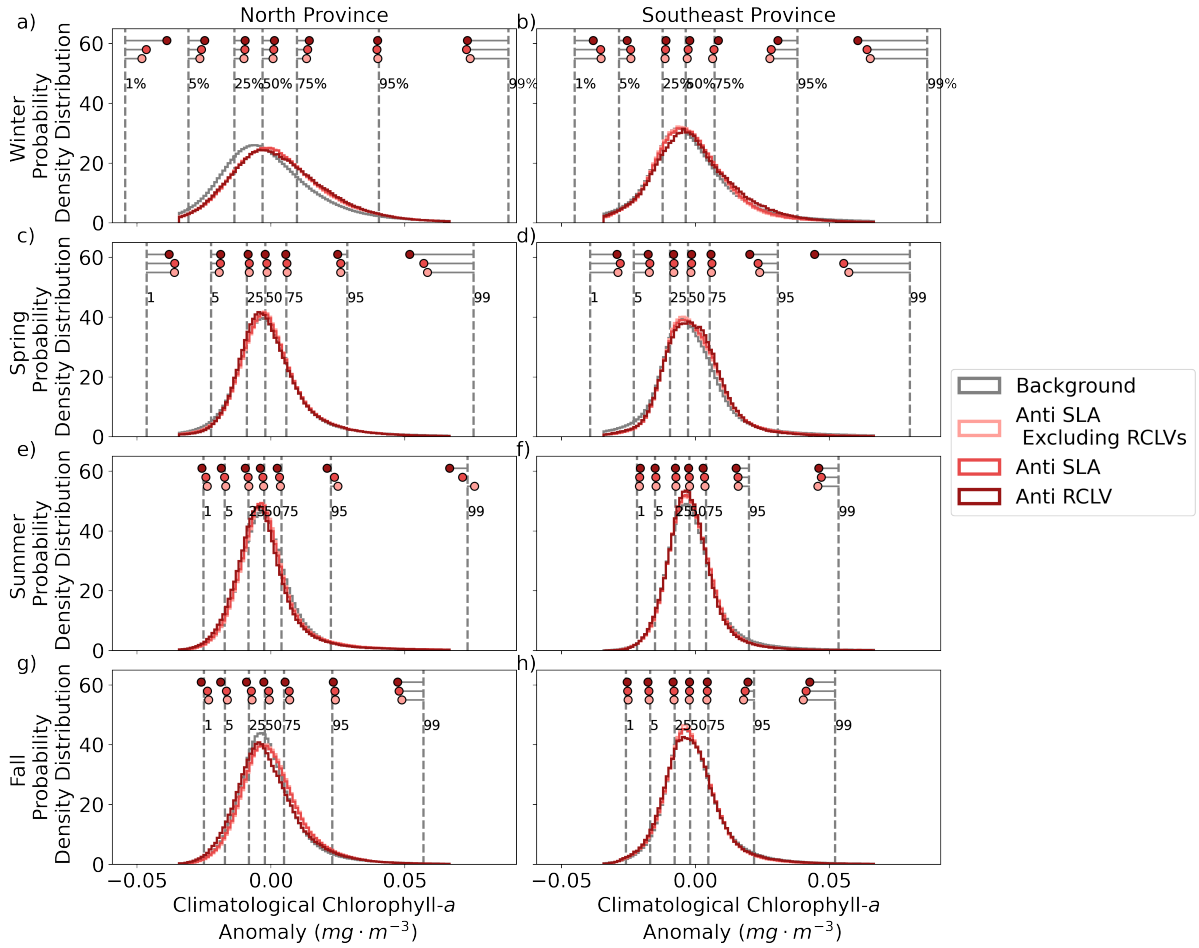

Figure S8. Probability density distributions of the climatological chl-a anomaly for anticyclonic eddies in the north and southeast provinces. The vertical dotted gray lines depict the quantiles of the distribution of the background for that province and season, and the dots show the equivalent quantiles for each eddy category.

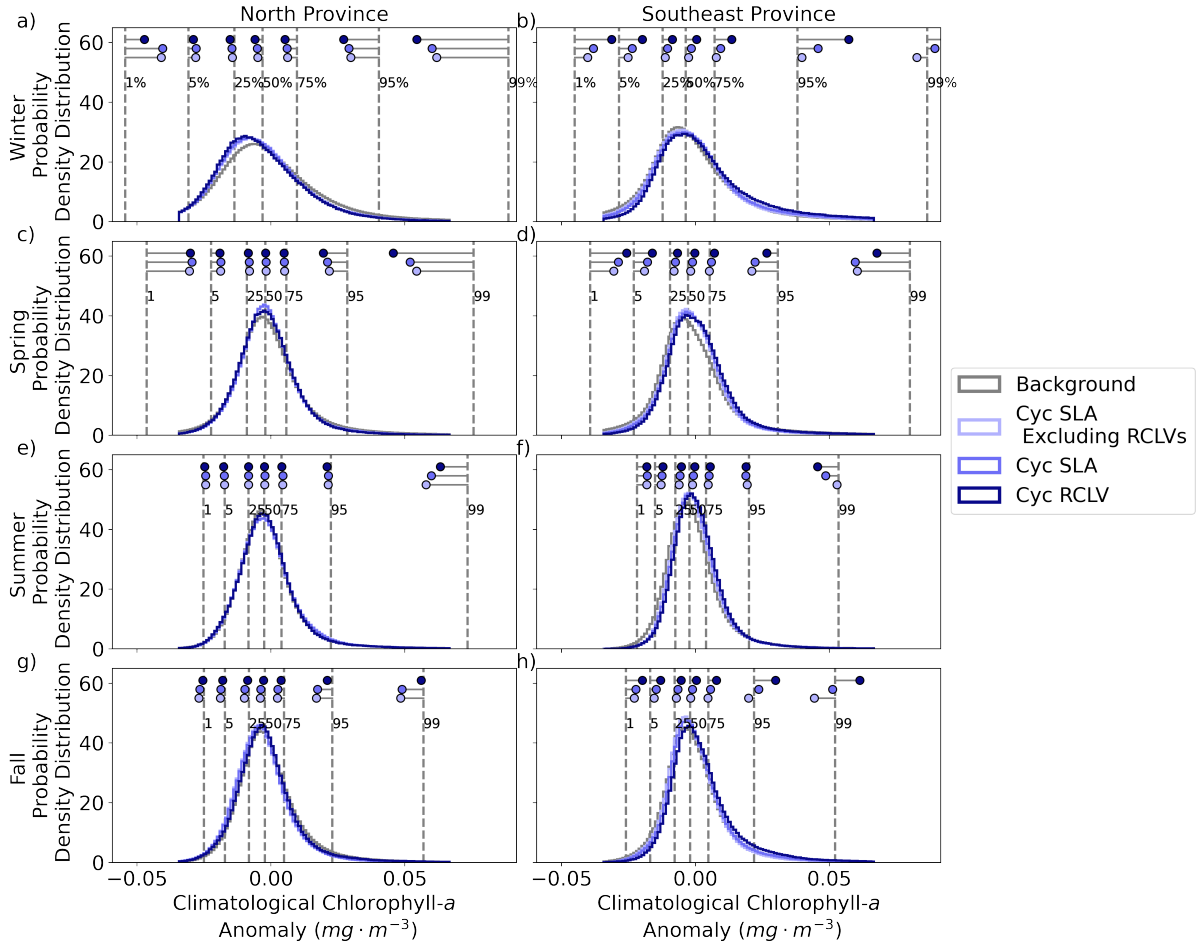

Figure S9. Same as Figure S8 but for cyclonic eddies.

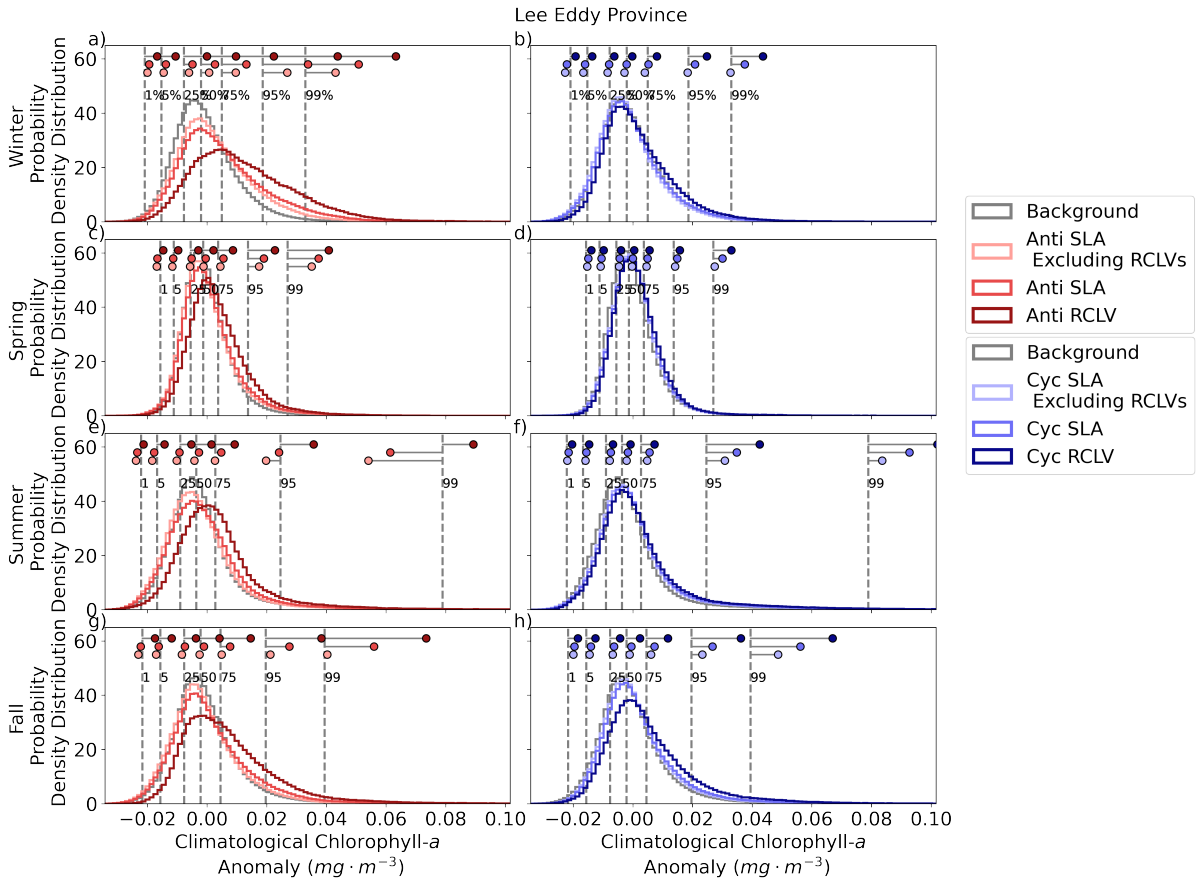

Figure S10. Same as Figure S8 and S9 but for the Hawaiian lee eddies.

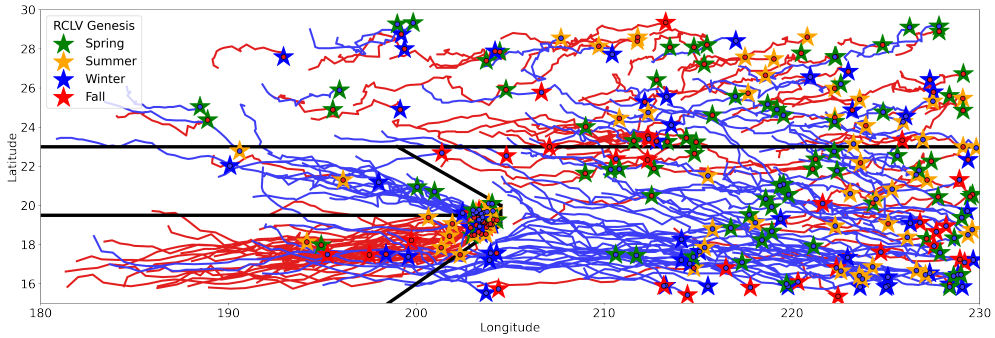

Figure S11. Trajectories of the eddy centers for long-lived (150+ day) RCLVs from 2000-2019. The cyclonic trajectories are in blue and the anticyclonic trajectories are in red. The dots and stars show the location of the eddy genesis, where the stars are color-coded by the birth season. The black lines show the boundaries of the mesoscale provinces used for the analysis in this study.

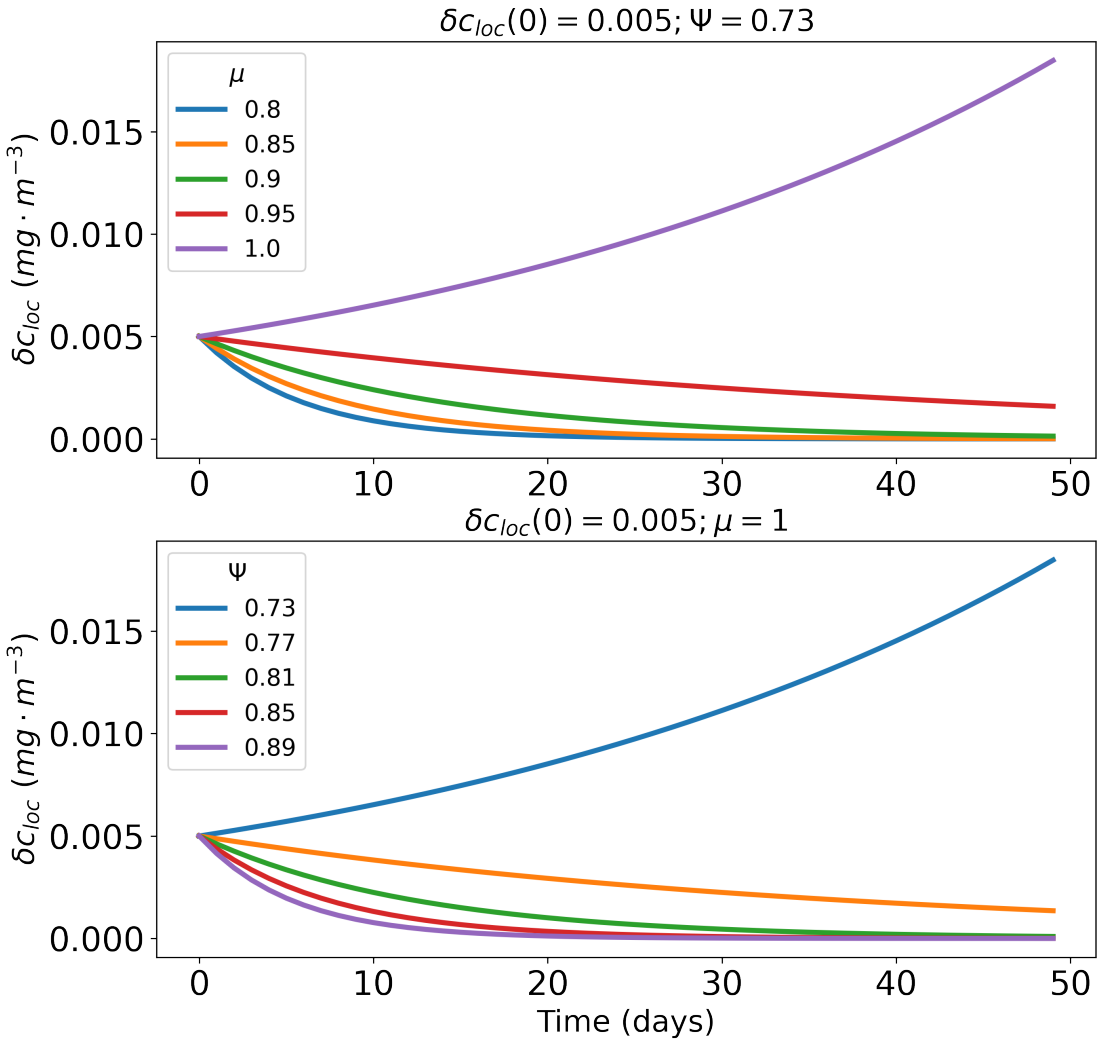

Figure S12. Solutions for Equation 8 of the main text. The top panel varies μ while holding Ψ constant, and the bottom varies Ψ while holding μ constant.

Text S1.

Equation 8 in the main text is a linear, 1st-order differential equation with the solution

$$\delta c_{loc}(t) = \delta c_{loc}(0) e^{(\mu_{in} - \frac{4}{3}\Psi)t} \tag{1}$$

where $c_{loc}(0)$ is the initialization time. In Figure S12, we tested this model by holding the lateral exchange rate Ψ constant and varying the biological rate of change μ, and vice versa. We find that both a high μ and a low Ψ is needed in order to have an increase in c_{loc} with time.